Special Collection

An *Ortho*-Tetraphenylene-Based "Geländer" Architecture Consisting Exclusively of 52 sp^2-Hybridized C Atoms

Hervé Dekkiche,[a, b] Juraj Malinčik,[a] Alessandro Prescimone,[a] Daniel Häussinger,[a] and Marcel Mayor*[a, b, c, d]

In memory of our friend and supporter François Diederich.

Abstract: A new type of "Geländer" molecule based on a *ortho*-tetraphenylene core is presented. The central *para*-quaterphenyl backbone is wrapped by a 4,4′-di((*Z*)-styryl)-1,1′-biphenyl banister, with its aryl rings covalently attached to all four phenyl rings of the backbone. The resulting helical chiral bicyclic architecture consists exclusively of sp^2-hybridized carbon atoms. The target structure was assembled by expanding the central *ortho*-tetraphenylene subunit with the required additional phenyl rings followed by a twofold macrocyclization. The first macrocyclization attempts based on a twofold McMurry coupling were successful but low yielding; the second strategy, profiting from olefin metathesis, provided satisfying yields. Hydrogenation of the olefins resulted in a saturated derivative of similar topology, thereby allowing the interdependence between saturation and physico-chemical properties to be studied. The target structures, including their solid-state structures, were fully characterized. The helical chiral bicycle was synthesized as a racemate and separated into pure enantiomers by HPLC on a chiral stationary phase. Comparison of recorded and simulated chiroptical properties allowed the enantiomers to be assigned.

Introduction

Spiral objects are ubiquitous in our life. While, in some cases, the spiral shape is crucial for the object's function (e.g., springs, the spiral growth of trees), there are plenty examples with the helical arrangement as an exclusively pleasing design element (e.g., ornaments on furniture, spiral columns). A similar dualism is found on the molecular level. The spiral spatial arrangement of biopolymers like DNA and proteins interacts with their chemical functions, while synthesized spiral molecules are first aesthetically appealing, but might have interesting chemical and physical properties due to their helical shape too,[1–3] resulting in promising applications.[4–8] Of particular interest are helically arranged π-systems, resulting in chiroptical properties like circular dichroism (CD) and circularly polarized photoluminescence (CPL). Due to their interaction with light, such structures become interesting elements of opto-electronical devices, for example as receptors/emitters of polarized light,[9,10] molecular switches[11] or probes for chiral molecules.[9,12,13] Recent developments profiting from the spin of the charge carrier to process information might even expand the application potential of conjugated chiral molecules as active elements for chirality induced spin selectivity (CISS).[14,15]

The most popular and widely studied helically arranged π-systems are helicenes (Figure 1a).[16] Their extended spiral π-system results in intense chiroptical activities with high extinction coefficients (e.g., $\Delta\varepsilon_{max}$ of 260 $L \cdot mol^{-1}$ for [6]-helicene).[17] Recent progresses in this field include the synthesis of multi-branched-helicenes[18] and helicenes with extended delocalization,[19–21] which both show unique properties. An appealing feature of larger helicenes is the in tegrity of their helical arrangement. For example, already the activation energy for the enantiomerization of the archetypical [6]-helicene corresponds with about 151.5 $kJ \cdot mol^{-1}$ at 25 °C[22,23] to a half-live time of ~10^6 years in the racemization process (page SI-86 in the Supporting Information). Their stability as enantiomer is not only favorable for enantiopure synthetic strategies, but also a requirement as active materials in chiroptical devices.

[a] Dr. H. Dekkiche, J. Malinčik, Dr. A. Prescimone, Prof. Dr. D. Häussinger, Prof. Dr. M. Mayor
Department of Chemistry, University of Basel
St. Johanns-Ring 19, 4056 Basel (Switzerland)
E-mail: marcel.mayor@unibas.ch

[b] Dr. H. Dekkiche, Prof. Dr. M. Mayor
NCCR Molecular Systems Engineering
BPR 1095, Mattenstrasse 24a, 4058 Basel (Switzerland)

[c] Prof. Dr. M. Mayor
Institute for Nanotechnology (INT)
Karlsruhe Institute of Technology (KIT)
P. O. Box 3640, 76021 Karlsruhe (Germany)

[d] Prof. Dr. M. Mayor
Lehn Institute of Functional Materials (LIFM)
School of Chemistry
Sun Yat-Sen University (SYSU)
Guangzhou 510275 (P.R. of China)

Supporting information for this article is available on the WWW under https://doi.org/10.1002/chem.202101968

Special Collection This article belongs to a Joint Special Collection dedicated to François Diederich.

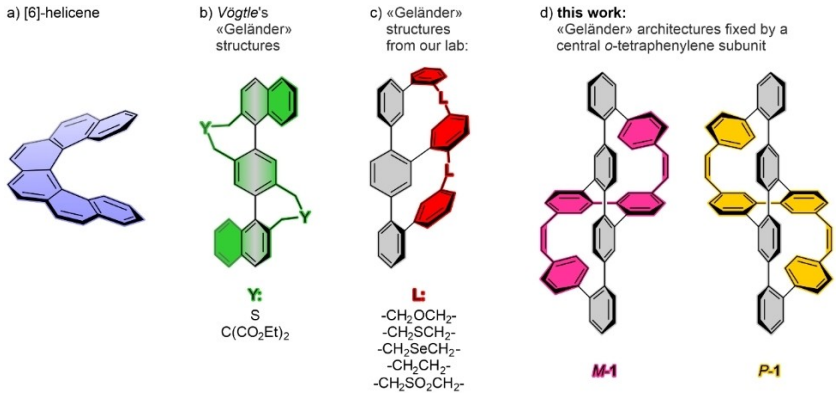

Figure 1. Model compounds with helically arranged subunits. The helically wrapped structures are colored, the molecule's backbone, which acts as an axle, is in grey.

An alternative approach towards helical structures are "Geländer" molecules, developed by Vögtle and co-workers more than 20 years ago (Figure 1b).[24] Axial chirality emerges from the interlinking of the phenyl rings of a *para*-terphenyl, with the latter as axle of the molecule and the interlinking structure wrapped helically like the bannister (German: *Geländer*) of a spiral staircase. These pioneering Geländer structures not only interconvert between enantiomers easily, the combination of the molecule's symmetry with the independence of both interlinking junctions also allows their *meso* forms, having opposed axial chirality along the molecule's axis. We developed the concept of Geländer molecules further by attaching a second phenyl-based oligomer of different step-size alongside the *para*-terphenyl axle (Figure 1c).[25–29] While the improved molecular design avoids *meso*-forms by propagating the axial chirality along the oligomers backbone, it came at the prize of considerably increased synthetic challenges. Furthermore, also these improved Geländer structures enantiomerize at room temperature and are thus rather model compounds to investigate the parameters controlling their racemization than stable enantiopure materials for chiroptical applications.

Herein, we present an alternative strategy to stable «Geländer»-type structures comprising a central *ortho*-tetraphenylene subunit (Figure 1d). The chirality emerges from the spatial arrangement of the four phenyl rings in this central building block, as the two adjacent biphenyl moieties can arrange in a right- or left-handed fashion relative to each other. Even so the racemization barrier of *ortho*-tetraphenylene is very high with decomposition prior to inversion reported for the parent structure at ambient pressure, it can theoretically interconvert between its *P* and *M* forms.[30,31] Recently new synthetic routes have been reported providing more elaborated structures from simple building blocks.[32,33] Double-helical (metallo)[34]-oligomers[35] and other interesting materials[32] based on this subunit have been reported lately.

To combine the structural features of Geländer molecules with the inherent chirality of *ortho*-tetraphenylene should be straightforward. As sketched in Scheme 1, the extension of the central *ortho*-tetraphenylene subunit with a pair of additional *ortho*-biphenyl units (blue in A, Scheme 1a) already provides the precursor of the target structure. Decorated with suitable functional groups (FG in Scheme 1a) at the end of both axis, double macrocyclization provides the intertwined molecular target **1**.

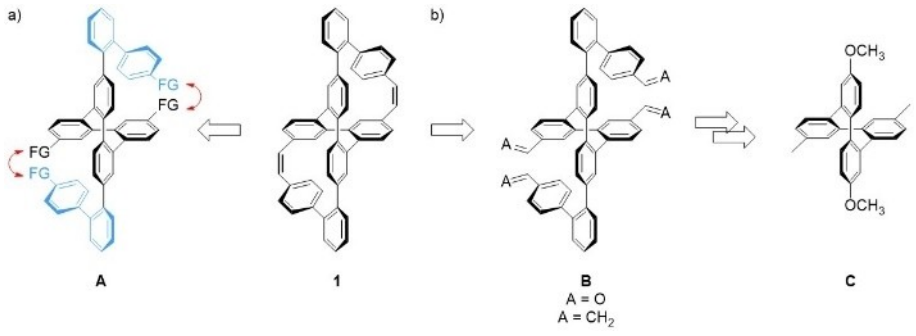

Scheme 1. Synthetic strategy to the mechanically locked Geländer molecule **1** (for clarity only the *M* enantiomer is displayed). a) Fundamental structural considerations. b) Fragmentation into suitable precursors.

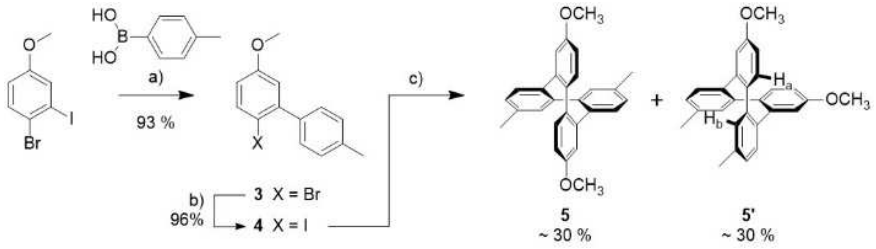

Scheme 2. Synthesis of *ortho*-tetraphenylene building block **5**. a) K_2CO_3, $Pd(PPh_3)_2Cl_2$ (cat.), THF/MeOH (4:1), reflux, overnight (argon); b) *n*BuLi then I_2, THF, −78 °C to RT, 1.5 h (argon); c) $NaHCO_3$, $Pd(OAc)_2$ (cat.), DMF, 110 °C, 1.5 d (air).

Results and Discussion

Synthetic strategy

The synthetic strategy has already been mentioned above in the introduction and is displayed in Scheme 1. The extension of the structure by two suitably functionalized *ortho*-biphenyl subunits (blue in Scheme 1a) brings both ring closing functional groups (FG in Scheme 1a) in close spatial proximity and thus, intramolecular ring closing was hypothesized to be favored compared to intermolecular coupling reactions. An interesting feature from a structural view-point is that the double macrocyclization locks the spatial arrangement of the system mechanically, further stabilizing the obtained enantiomers. Of particular interest will be the optical features pointing at the degree of delocalization of the π-systems in the target structure **1**, with a framework consisting exclusively of sp^2-hybridized carbon atoms.

As sketched in the octaphenyl derivative **B** in Scheme 1b, aldehydes or olefins were considered as functional group for the intended macrocyclizations. With the tetra-aldehyde precursor an intramolecular McMurry coupling[36,37] was considered as cyclization step, while olefin metathesis[38] was the method of choice for the tetraolefin precursor. As Wittig chemistry[39,40] enables to obtain the tetra-olefin precursor from the tetra-aldehyde precursor, the latter became the main objective of the synthetic strategy. An ideal *ortho*-tetraphenylene precursor would be **C**. Its methoxy groups should be easily transformable to leaving groups providing the central building block to attach the suitably functionalized *ortho*-biphenyl subunits by Suzuki-Miyaura coupling chemistry.[41,42]

Synthesis of building blocks and precursors

For the synthesis of the *ortho*-tetraphenylene backbone targeted in this study, a procedure involving the oxidative coupling of a iodobiphenyl derivative was chosen.[43] Compared to other routes involving the formation of reactive organometallic species and more sophisticated intermediates,[33] this catalytic reaction offers the advantage of using simple conditions while providing good yields of the desired product. Nevertheless, due to the quite harsh reaction conditions required, exclusively robust functional groups are acceptable in the substrate. Thus methoxy and methyl decorated precursors were considered as displayed in Scheme 2.

Starting from commercially available *p*-tolylboronic acid and home-made 4-bromo-3-iodoanisole, the intermediate **3** was obtained in 93% yield following standard Suzuki-Miyaura coupling reaction conditions. The iodo-derivative **4** could then be obtained in almost quantitative yield by bromine-lithium exchange and subsequent quenching with iodine. Treatment of **4** with catalytic amounts of $Pd(OAc)_2$ and a slight excess of $NaHCO_3$ in DMF at 110 °C for more than a day provided the *ortho*-tetraphenylenes **5** and **5'** in a yield of about 60% over both structural isomers. Despite their comparable polarity, both isomers were successfully separated by column chromatography (CC). The desired central building block **5** was isolated in 30% yield, which is in good agreement with the data reported previously for similar compounds.[43] As both structural isomers **5** and **5'** have very comparable ^{1}H NMR spectra, their differentiation was only possible due to the close proximity of H_a and H_b in **5'** observed in the NOESY spectrum, which is not the case in **5** (Figures S2-1 and S2-2). The NOESY spectra further allowed two sets of three signals to be assigned for the two phenyl rings of the *ortho*-tetraphenylene moiety.

The central building block **5** was further developed (Scheme 3) by removing the methyl protection groups with boron tribromide to yield **6** exposing two phenolic hydroxy groups in quantitative yields. The latter was subsequently transformed into the bis-triflate **7** by treatment with trifluoromethanesulfonic anhydride in basic conditions. CC provided **7** in very good 86% yield as white powdery solid. The formation of **7** was monitored by ^{19}F NMR, where a signal at −72.91 ppm

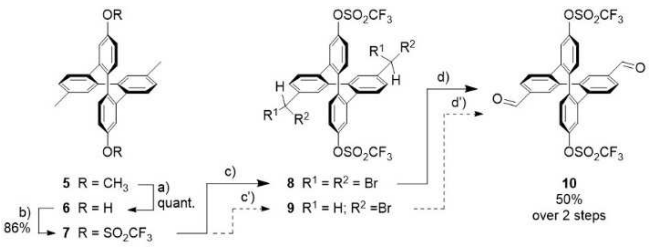

Scheme 3. Synthesis of building-block **8**. a) BBr_3, CH_2Cl_2, −78 °C to RT, overnight; b) Tf_2O, pyridine, CH_2Cl_2, RT, 1.5 h; c) NBS, BPO (cat.), CCl_4, reflux, 4–5 h; d) DMSO, 100 °C, overnight; c') reaction with 2 equiv. NBS; d') hydrolysis, then oxidation.

indicated the presence of aromatic triflates. To transform both methyl groups of **7** into aldehydes, we considered first a route via the benzylic bromide **9**, which could be hydrolyzed to the benzylic alcohol and oxidized to the desired aldehyde **10** (dashed arrows in Scheme 3). However, the controlled mono-bromination of both methyl groups with a slight excess of *N*-bromosuccinimide (NBS) turned out to be challenging and the apparently almost statistical formation of multi-brominated species not only handicapped the yield, but also rendered isolation and purification of **9** laborious. We thus decided to profit from the compounds tendency for multiple bromination and treated **7** with a slight excess of NBS (4.2 equiv) to obtain the tetrabrominated compound **8**. Due to the remaining variety of brominated species, also the isolation of **8** turned out to be challenging and ineffective. Thus the crude reaction mixture was kept overnight in 100 °C hot DMSO to transform the dibromo methyl groups into aldehydes,[44] and after work-up and CC, the dialdehyde **10** was obtained in reasonable 50% yields over both steps. The course of the reaction was monitored by ^{1}H NMR spectroscopy, where the raise of the unshielded aldehyde-H signal at 10.04 ppm at the cost of the dibromobenzyl-H at 6.64 ppm was indicative for the aldehyde formation.

Following our synthetic strategy, a suitably functionalized biphenyl building block was required to develop the precursor (**14**) for the macrocyclization. As displayed in Scheme 4, the biphenyl scaffold was obtained by exposing 2-(4-iodophenyl)-1,3-dioxolane and 2-bromophenyl boronic acid to typical Suzuki-Miyaura coupling conditions. To profit from the superior reactivity of aryl iodides compared to aryl bromides, the THF/methanol solvent mixture was chosen to avoid reaction temperatures above 65 °C. After work-up and CC, the biphenyl **11** was isolated as colorless oil in 80% yield. The bromine substituent of **11** was transformed into a pinacol ester of the corresponding boronic acid by a lithium bromine exchange with *n*-butyllithium, and subsequent quenching with isopropyl pinacol borate. The boronic acid derivative **12** was isolated in quantitative yields by CC. Treatment of **12** in acidic conditions (*para*-toluenesulfonic acid (PTSA) in an acetone-water mixture) provided the aldehyde **13** in 90% isolated yield. In spite of the sensitivity of the pinacolborate substituent, neither impurities nor degradation products were detected in the ^{1}H and ^{13}C NMR spectra of building block **13**.

With both building blocks in hand, the *ortho*-tetraphenylene bis-triflate **10** and the biphenyl pinacolborate **13**, the assembly of the octa-aryl precursor **14** was considered (Scheme 4). For the Suzuki-Miyaura type coupling, reported conditions were adapted.[45] Thus the bis-triflate **10** was treated with 2.4 equivalents of the pinacolborate **13** in the presence of tetrakis (triphenylphos-phine)palladium(0) as catalyst and 5 equivalents of tripotassium phosphate monohydrate as base for several hours at 85 °C. After work-up, the tetra aldehyde advanced precursor **14**, already comprising all the carbon atoms of the target structure, was isolated in very good 86% yield after CC as white powder. The characteristic feature in the ^{1}H NMR spectrum of **14** are the two distinct aldehyde-H signals at 10.02 and 9.99 ppm respectively.

Macrocyclization to the conformationally locked structure

The efficient synthetic availability of the tetra aldehyde precursor **14** enabled the exploration of macrocyclization conditions. According to our synthetic strategy, a twofold intramolecular McMurry reaction was considered first (Scheme 5). Due to lack of in depth experience, the used reaction conditions were inspired by protocols applied to aryl-aldehydes[46] and enabled intramolecular cyclizations.[47] Thus the tetra aldehyde **14** dissolved in THF was added to a 0 °C cold solution of titanium tetrachloride ($TiCl_4$, 4 equiv) and zinc dust (Zn, 12 equiv) under an argon protection gas atmosphere. After refluxing the reaction mixture for about 16 h and work up, the desired doubly cyclized target structure **1** was isolated in 8.5% yield by CC.

Even so the central *ortho*-tetraphenylene structure hardly enantiomerizes at room temperature, the twofold intramolecular ring closing further reinforces mechanically the final enantiomeric form adopted by the molecule. The presented reactions sequence provides the mechanically fixed target structure **1** as racemate, but for clarity only the *M* enantiomers are displayed in the following synthetic schemes.

We were excited that in spite of the low yield, the small amount of **1** could easily be isolated from the remaining ingredients of the reaction mixture by CC due to its nonpolar nature. However, in spite of numerous efforts, the yield of the reaction could not be improved and remained below 10%. To

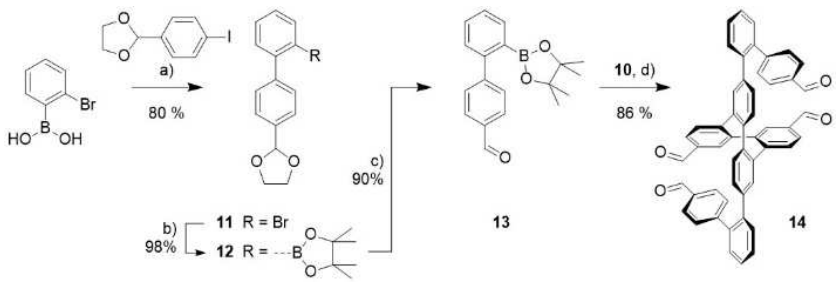

Scheme 4. Synthesis of the biphenyl building-block **13** and its merger with the *ortho*-tetraphenylene **10** forming the advanced precursor **14**. a) K_2CO_3, $Pd(PPh_3)_2Cl_2$ (cat.), THF/MeOH (4:1), reflux, 4 h (argon); b) *n*BuLi then *i*PrB$_{pin}$, THF, −78 °C to RT, 1.5 h (argon); c) PTSA, acetone/water (10:1), RT, overnight; d) $K_3PO_4 \cdot H_2O$, $Pd(PPh_3)_4$, dioxane/water (5:1), reflux, overnight (argon).

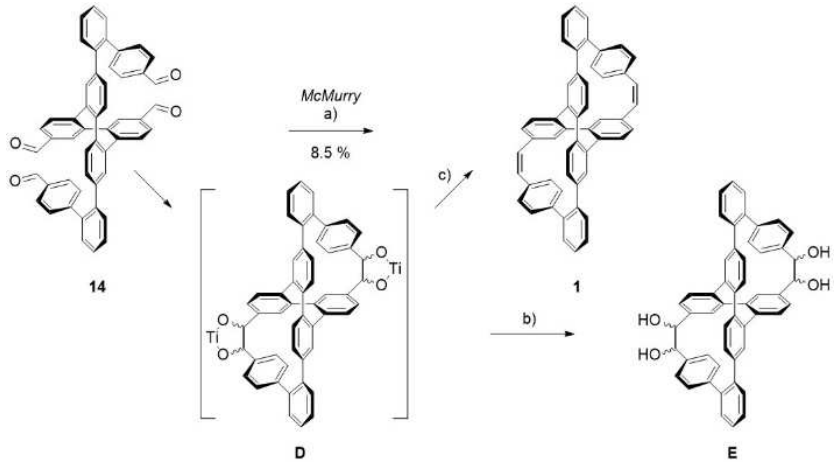

Scheme 5. Synthesis of the mechanically locked Geländer molecule **1**, part I: Intramolecular macrocyclizations by McMurry reactions (for clarity, only the *M* enantiomers are displayed). a) $TiCl_4$ and Zn, THF (high-dilution), 0 °C to reflux, overnight, under Ar; b) quenching with $NH_4Cl_{(aq.)}$ after 30 min at 0 °C; c) heating overnight.

figure out the origin of the yield limitation in this McMurry macrocyclization approach, efforts were made to identify the reaction intermediates. Thus the reaction was performed on a smaller scale and part of it was quenched with NH_4Cl after 30 min reacting with the $TiCl_4$/Zn couple at 0 °C.

According to the analysis by matrix-assisted laser desorption-ionization mass spectrometry (MALDI-MS, Figure S2-4), all the starting material was consumed forming exclusively the tetra-hydroxy derivative **E** in Scheme 5 (*m/z* peak of 743.552 corresponding to $[M+H_3O]^+$). Even so a single signal was recorded in the MALDI-MS analysis, a cluster of several peaks was detected in the high performance liquid chromatography (HPLC) analysis of the reaction mixture (Figure S2-3). This group of peaks of different intensity is expected considering the variety of possible diastereomers emerging from the spatial arrangements of the 4 hydroxy groups (in theory there are 10 enantiomeric pairs of diastereomers possible, see Figure S2-5). After refluxing the intermediate **D** overnight, the formation of the target structure **1** together with a variety of other more polar derivatives is observed. Considering the mechanism of the McMurry coupling and the variety of diastereoisomers detected after the quenching of the intermediate **D**, it is tempting to hypothesize that only some of the formed double titanium diastereoisomers **D** are able to degrade properly to the desired bis-olefin **1**, while the remaining ones are most likely decomposing into structures exposing hydroxyl groups considering their increased polarity compared to the target structure.

While the rational for the limited yield for the double macrocyclization by McMurry reaction is intellectually satisfying, it does not improve the acceptability of the yield. Considering the perfect preorganization of both aldehydes, an efficient ring closing was expected. A twofold ring-closing metathesis (RCM) reaction was thus considered as alternative. Therefore, the tetra-aldehyde **10** was converted first into the tetra-vinyl derivative **15** in good yield by reaction with methyltriphenylphosphonium bromide using standard Wittig reaction conditions (Scheme 6). The formation of **15** was monitored by ^{1}H NMR, where two sets of vinylic protons at 6.74, 5.76 and 5.28 ppm and 6.65, 5.69 and 5.21 ppm (see Figure S1-17 for the COSY spectrum) appeared. With the tetra-vinyl precursor **15** in hands, the RCM was performed with the Hoveyda-Grubbs second-generation catalyst[48,49] (20 mol%) using high-dilution conditions in refluxing dichloromethane.[50] The reaction was monitored by MALDI-MS (Figures S2-6 and S2-7) revealing that

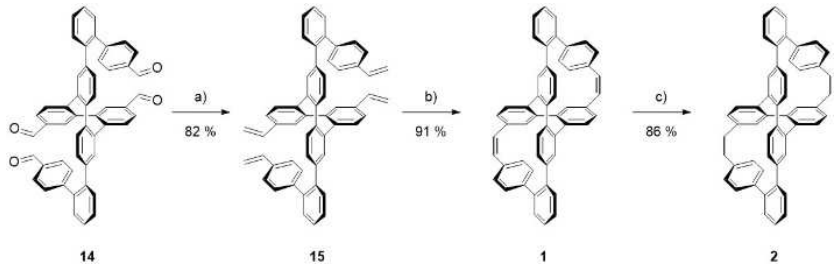

Scheme 6. Synthesis of the mechanically locked Geländer molecule **1**, part II: Intramolecular macrocyclizations by RCM and reduction to the saturated derivative **2** (for clarity, only the *M* enantiomers are displayed). a) $MePPh_3Br$, *n*BuLi, THF, 0 °C to RT, overnight (argon); Hoveyda-Grubbs second-generation. (cat.), CH_2Cl_2 (high-dilution), reflux, overnight; c) 1,4-cyclohexadiene, Pd/C, dioxane, 90 °C (sealed tube), 1.5 h (argon).

the stepwise transformation of the starting material into the desired bicyclic **1** was almost complete after 6 h. After 24 h traces of partially closed intermediate remained constantly and the reaction was worked-up. To our delight, the racemate of the mechanically fixed bicyclic Geländer structure **1** was isolated in very good 91% yield after CC. The considerably improved availability of **1** even allowed for further derivatization. As obvious first example, both double bonds of **1** were hydrogenated to provide the saturated analogue **2**. For this transformation, **1** was treated with 1,4-cyclohexadiene in 90 °C hot dioxane in the presence of catalytic amounts of palladium on carbon (Pd/C). After work-up and CC the saturated bicyclic structure **2** was isolated in 84% yield.[51]

All new compounds were fully characterized by ^{1}H and ^{13}C NMR spectroscopy and high resolution mass spectrometry. The identity of both bicyclic target structures **1** and **2** was further corroborated by their solid-state structures. Single crystals suitable for X-ray diffraction analysis were obtained by slow diffusion of methanol vapor into a CH_2Cl_2 solution of racemic **1** and into a chloroform solution of racemic **2**. Furthermore, the racemic mixtures of **1** and **2** were separated into enantiomers by preparative HPLC with a chiral stationary phase (Chiralpak IB–N, Figures S2-8 and S2-9).

Physico-chemical characterization

NMR spectroscopy: The comparison of the physico-chemical properties of both cyclized target compounds **1** and **2** was of particular interest. Both bicyclic structures have very comparable geometrical topology, but differ in their composition. While **1** consists exclusively of sp^2-hybridized carbon atoms, the saturated ethylene linkers in **2** consist of sp^3 carbons, adding not only four additional hydrogen atoms, but also some increased flexibility of the structural scaffold. TOCSY (Figures S1-14, S1-19, and S1-20) and NOESY (Figures S1-15, S1-21, and S1-22) experiments with a 600 MHz NMR-spectrometer enabled the assignment of all ^{1}H signals of both bicycles **1** and **2** (Figures 2 and S2-10).

Clearly the resonances of the hydrogen atoms of the interlinking structures differ between both bicycles. While the hydrogens (H15 and H16 in Figure 2) of the ethen-1,2-diyl linker of **1** resonate at 6.78 and 6.89 ppm and display the expected ~10 Hz coupling of vicinal *cis* olefin hydrogens, the H-atoms (H15-H18 in Figure 2) of the ethan-1,2-diyl linker of **2** are observed as complex multiplex signals at 2.65 and 3.12 ppm respectively. Interestingly, the coupling between all four nuclei combined with their locked arrangement results in a unique multiplicity pattern. Apart from this expected variation in the spectroscopic signature, the signals of the oligoaryl scaffold remain essentially the same between both bicycles. Almost all aryl hydrogens display minute to small up-field shifts upon the transition from **1** to **2**, with the exception of H11 (highlighted light blue in Figure 2) which shifts from 6.10 ppm in **1** to 6.17 ppm in **2** (blue arrow in Figure 2). The expected increase in flexibility by going from **1** to **2** is hardly detectable in the NMR spectra. The only indications are small increases in the intensity of weak NOESY signals between hydrogens of neighboring aryl systems, such as H14 of the biphenyl system and H8 of the central *ortho*-tetraphenylene scaffold or H11 and H6.

Over all, based on the NMR spectra of both compounds **1** and **2**, only minor structural variations were observed upon hydrogenation of the interlinking olefins. An in-depth analysis of the spatial rearrangements within the bicyclic scaffold triggered by this transformation was possible based on their solid-state structures.

X-ray structures: Both racemates **1** and **2** crystalize in a monoclinic space group with unit cells comprising 3 and 2 sets of enantiomeric pairs respectively (see Figures S2-11 and S2-12 for packing views). In spite of the comparable spatial arrangement of their molecular subunits and the fact that both single crystals were obtained from a similar solvent system, they

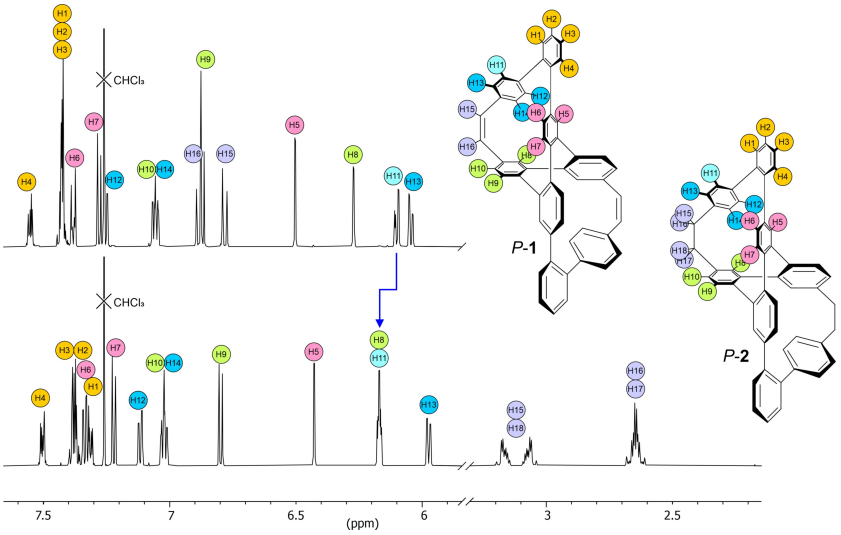

Figure 2. ^{1}H NMR spectra of racemic **1** (top) and racemic **2** (bottom) with assignment of the signals (only the *P* enantiomers are displayed for the assignment). The blue arrow shows H11 (cyan) to be the only hydrogen atom experiencing a downfield shift on going from **1** to **2**.

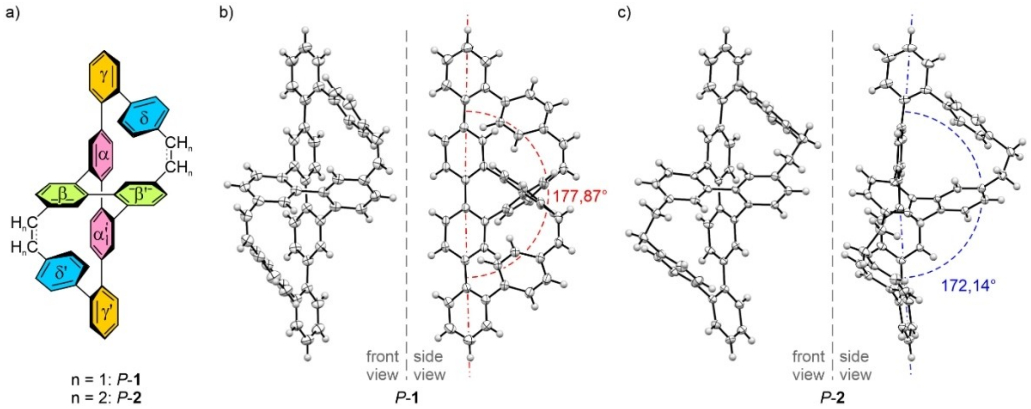

Figure 3. a) Labeling of the aryl rings in the bicyclic oligo-aryl scaffold of **1** and **2** to aid discussion of the inter-aryl torsion angles. Solid-state structures of the *P* enantiomers of b) **1** and c) **2** as ORTEP plots with 50% probability. The backbone axes (dot and dash lines) are divided in the upper and lower biphenyl system of the terphenyl backbone to analyze the deviation from linearity of the molecular backbone.

crystalize in slightly different space groups (*C*2/*c* for **1** and $P2_1/c$ for **2**). To analyze the effects caused by the saturated ethylene bridge in **2**, the torsion angles between the aryl rings and along the two C atoms of the bridging units were measured. The labeling of the aryl subunits as α, β, γ, and δ is sketched in Figure 3a, and the recorded torsion angles are listed in Table 1. Unsurprisingly, the largest change in torsion angle was observed for the pair of carbon atoms interlinking the biphenyl subunit with the central *ortho*-tetraphenylene subunit, for which the two-vicinal olefin *Z* substituents of the scaffold of **1** were with a torsion angle of 5.63° bent only marginally out of the plane. This suggests that in spite of the rigidity emerging from the fixation in a bicyclic architecture, the oligo-aryl scaffold provides enough degrees of freedom allowing the arrangement of the bicycle **1** consisting exclusively of sp^2-hybridized carbon atoms without too much strain. The adaptability of the oligo-aryl scaffold is further demonstrated by the saturated derivative **2**, which comprises two pairs of sp^3-hybridized C-atoms as interlinking units. The torsion angle along the C–C single bond is with 58.74° considerably larger compared to **1** (5.63°), and the bond length between both atoms increases from 1.335 Å for the C=C bond in **1** to 1.539 Å for the C–C bond in **2**. The 50.65° torsion angle resembles the 60° angle between vicinal hydrogen substituents of the most stable staggered conformation of ethane and again, it seems that the oligo-aryl scaffold is able to intercept structural modifications by adapting the torsion angles between the aryl subunits.

Table 1. Torsion angles measured between the different aryl rings and along the interlinking pair of C-atoms in the solid-state structures of **1** and **2**. In the case of **2**, mean torsion angles adopted by the phenyl rings of both, the upper and lower parts of the molecule are presented.

	Tetraphenylene backbone			Other structural features		
Torsion angle	$\alpha\alpha'$	$\beta\beta'$	$A\beta$	$\alpha\gamma$	$\gamma\delta$	CC
bicycle **1**	60.10°	68.56°	63.80°	65.52°	42.21°	5.63°
bicycle **2**	61.80°	66.41°	64.53°	71.12°	57.70°	50.65°

However, the inter-aryl torsion angles listed in Table 1 display rather small variations between both bicycles **1** and **2**. The structural perturbation caused by the hydrogenation of the double bond is adsorbed by small adjustments of all inter-aryl torsion angles ranging from +0.73° for $\alpha\beta$ to −2.15° for $\beta\beta'$. The only substantial variation is observed for $\gamma\delta$, for which most likely the steric interaction with the hydrogen atoms of the enthan-1,2-diyl linker are causing an increase of the torsion angle by 15.49°. Interestingly, the vertical axis of **2** (dot and dash blue line in Figure 3c) is by about 5.7° stronger bent compared to **1** (dot and dash red line in Figure 3b). At the first glance this is counterintuitive as the enthan-1,2-diyl linker in **2** is 0.204 Å longer than the ethen-1,2-diyl linker of **1**. However, the difference in length is more than compensated by the spatial arrangement of the C–C bond. While in the case of **1** the C=C bond is almost parallel to the vertical axis and deviates only by 3.2° from parallelism, the C–C bond of **2** is with a deviation of 34.7° from parallelism much less effective in bridging the gap between the subunits of the oligo-aryl scaffold.

The analyses of the solid-state structures on the whole corroborates the conclusions already drawn from the NMR experiments. Namely the transition from **1** to **2** mainly effects the structure of the bridging C-atom pair and has apart from that only marginal effects on the arrangement of the oligo-aryl scaffold.

Electronic properties: Of particular interest were the electronic properties of both bicycles **1** and **2**. Substituting the sp^2-hybridized carbon atom pairs by sp^3-hybridized ones removes the option of electronic communication between the interlinked aryl systems by π-conjugation, an effect which should be reflected in the electronic features of the compounds. The UV–vis spectra of racemic **1** and **2** are displayed in Figure 4a and b, respectively (purple solid lines with the corresponding *y*-axis on the right side). The UV spectra of both target compounds consist of broad structureless absorption bands with comparable maxima of their extinction coefficients between 5 and $6.10^4\ L \cdot mol^{-1}$. Their lowest energy transition only displays a

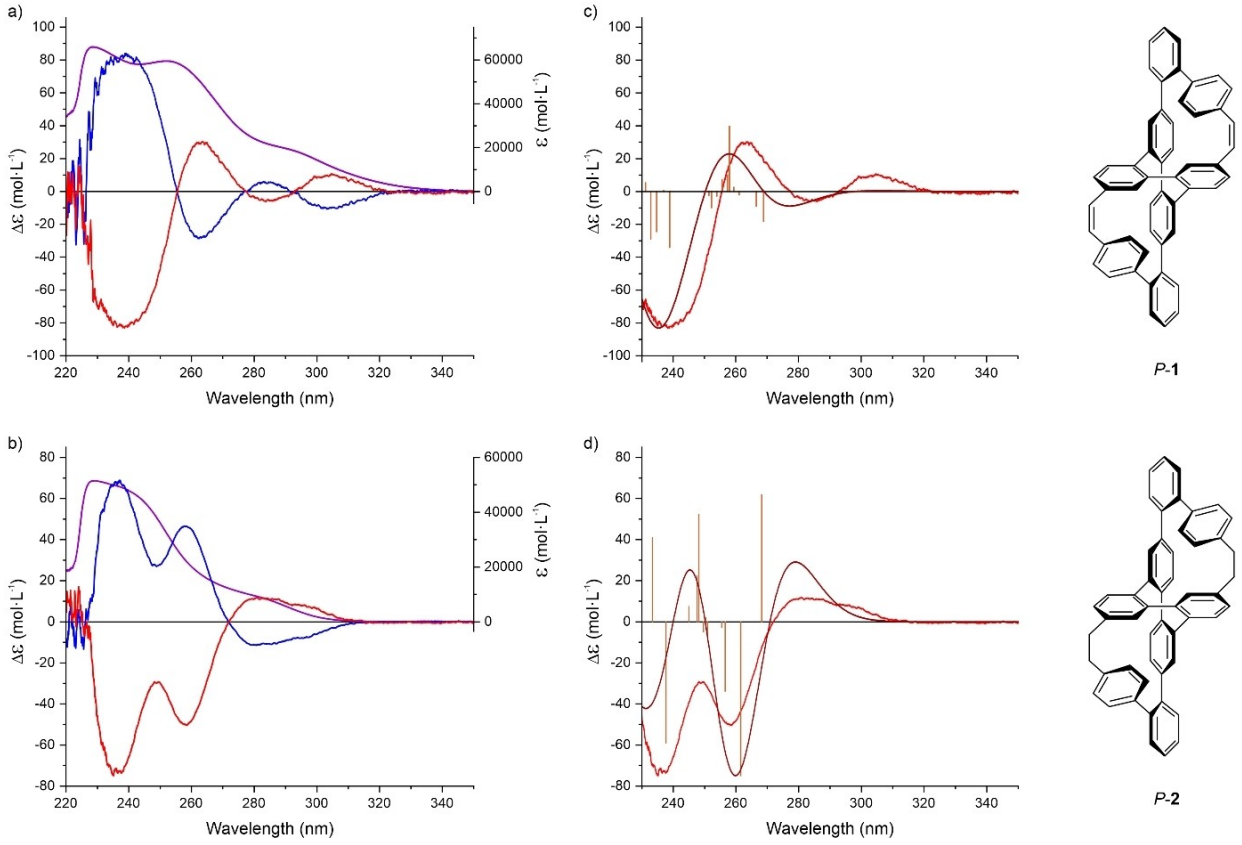

Figure 4. a), b) UV-vis (solid purple line, *y*-axis on the right side) and CD spectra of both enantiomers (*P* enantiomer: red line; *M* enantiomer: blue line) of **1** and **2** respectively. All spectra were recorded at 20 °C as 1×10^{-5} M solution in chloroform. c), d) Comparison of the simulated (dark red line) and the recorded (red line) CD spectra of the *P* enantiomers. The brown bars are the calculated first 50 electronic transitions which result in the simulated spectrum ($\varsigma = 0.25$ eV).

small bathochromic shift for **1** compared to **2** with values of 290 and 284 nm respectively. The most apparent difference between both UV spectra is the bathochromic shift of the second broad absorption band, which lies at 253 nm in the case of **1** and is observed as shoulder at about 240 nm for **2**. While the observed bathochromic shifts point at the expected slightly increased π-electron delocalization in **1**, the modesty of the effect is not surprising as the olefin π-system of the bridging pair in **1** is almost perpendicular to the neighboring aryl-π-systems reducing the efficiency of π-conjugation.

Pure enantiomers of both bicycles **1** and **2** were obtained by preparative HPLC with a chiral stationary phase (Chiralpak IB–N, Figures S2-8 and S2-9). All isolated enantiomers were stable compounds and did not display any racemization tendency even at elevated temperatures. The CD spectra of the pairs of enantiomers is displayed in Figure 4a and b for **1** and **2** respectively, with the blue line for the enantiomer with the shorter retention time in the chiral HPLC analysis for both cases. In the CD spectra of the enantiopure species, pairs of Cotton bands of opposite signs were observed at 239, 262, 285, and 305 nm for **1**, and at 237, 258, 282, and 300 nm for **2**. Comparable maximal $\Delta\varepsilon$ values were recorded around 240 nm for both bicyclic structures with 83 $L\cdot mol^{-1}$ for **1** and 68 $L\cdot mol^{-1}$ for **2**, resulting in similar dissymmetry factors (g_{CD}) of about $1.4\cdot10^{-3}$ at this wavelength (Figure S2-15). These $\Delta\varepsilon$ values are substantially higher than the ones measured for previously reported helical chiral Geländer molecules with terphenyl backbones,[28] or naphthol derivatives (10–20 $L\cdot mol^{-1}$),[52] but considerably smaller than the ones reported for more extended systems, such as a twisted cycloparaphenylene derivative (~200 $L\cdot mol^{-1}$).[53] While at first glance both bicyclic helical hydrocarbons **1** and **2** display absorptions of the same polarity for the same enantiomers, an inversion of the Cotton bands at 250–290 nm was recorded. The rather modest $\Delta\varepsilon$ and g_{CD} values further document the lack of π-conjugation in the helically wrapped oligo-aryl architectures.

In spite of numerous attempts, the crystallization of pure enantiomers was not successful for both structures. To assign the absolute configurations to the separated enantiomers, DFT-calculations were performed. The molecular structure of interest was optimized using the B3LYP-D3(BJ)/6-31 g(d) method, profiting from the coordinates of the corresponding enantiomer in the X-ray structures of the racemate as starting point. The corresponding CD spectra were obtained by using TD-CAM-B3LYP/6-31 g(d) and calculating the first 50 singlet excitations (brown bars in Figure 4c and d). Taking the *P* enantiomers as example, the resulting calculated CD spectra are displayed as dark red lines in Figure 4c and d for *P*-**1** and *P*-**2**, respectively. The simulated spectra fit well with recorded ones of the enantiomers with longer retention times (red lines in Figure 4c

and d) allowing the assignment of the separated enantiomers. Namely the *M* enantiomer as first eluting sample on the chiral stationary phase (Chiralpak IB–N, Figures S2-8 and S2-9) followed by the *P* enantiomer for both bicyclic structures **1** and **2**. The comparable behavior of both target structures on the chiral stationary phase was expected after structural analyses by NMR spectroscopy and X-ray diffraction already displayed rather moderate structural variations.

Additionally, the first molecular orbitals of both compounds **1** and **2** were calculated at the B3LYP/cc-pVTZ level of theory (Figures S2-16 and S2-17) and the main electronic transitions were calculated at the CAM-B3LYP/6-31 g(d) level of theory (Tables S1 and S2). In both cases, the lowest energy absorption observed in UV-vis (and therefore CD) spectroscopy can easily be attributed to a combination of the HOMO→LUMO and HOMO-1→LUMO+1 transitions. Though, as both HOMO and HOMO-1 and LUMO and LUMO+1 orbitals seems to be degenerated in the case of **1**, they are not in the case of **2**, most probably due to the different symmetry adopted by the molecule. The variations in the molecular orbitals energies (−0.224 eV for the HOMO-1 and −0.029 eV for the LUMO+1 of **2** compared to −0.216 and −0.041 eV respectively for **1**) can also be linked to the rupture of the conjugation through the linking C–C bond, and explain the bathochromic shift observed in electronic spectroscopy. Furthermore, the electronic transition analysis reveals that the most intense transition is related to the HOMO-1→LUMO+3 transition in the case of **1** and HOMO-2→LUMO+3 in the case of **2**.

Conclusion

Profiting from the rigid and stable arrangement of both biphenyl subunits in *ortho*-tetraphenylene, conformationally locked bicyclic "Geländer" architectures were assembled in 11 or 12 synthetic steps. The target structures **1** and **2** are hydrocarbons of which the first consists exclusively of sp^2-hybridized carbon atoms. Both bicyclic structures **1** and **2** were synthesized as racemic mixtures and were subsequently separated into pure enantiomers that do not racemize. The assembly was based on developing the suitably functionalized precursors **14** and **15** by functional-group transformations and C–C coupling chemistry, which subsequently underwent a twofold intramolecular macrocyclization. Initial attempts to transform the tetra-aldehyde **14** through McMurry coupling into bicycle **1** were successful, but led also to a variety of side products. The superior synthetic strategy was a twofold ring-closing metathesis reaction of the tetra-vinyl precursor **15**. Subsequent hydrogenation of both interlinking double bonds of **1** provided the ethan-1,2-diyl interlinked bicycle **2**. Structural analyses and comparison of both bicyclic Geländer structures **1** and **2**, revealed an oligo-phenyl scaffold with enough degrees of freedom to absorb the structural differences. Solid-state structures for both bicycles **1** and **2** were only available for the racemic mixture. However, a very good fit between simulated and recorded CD spectra allowed the assignment of the helical chiral enantiomers.

In summary, an efficient approach to helical chiral and enantio-stable model compounds is presented. The modular synthetic strategy allows further derivatization of the parent structures, enabling their optimization and integration into opto-electronic devices as chiroptical building blocks. We are currently exploring both the scope and limitation of *ortho*-tetraphenylene as a chirality-endowing subunit in carbon architectures.

Experimental Section

Synthesis of 1 from 14 (McMurry coupling strategy): A solution of $TiCl_4$ (1 M in CH_2Cl_2, 0.72 mL, 0.72 mmol, 4 equiv) was added to a suspension of Zn dust (140 mg, 2.16 mmol, 12 equiv) in dry THF (25 mL) at 0 °C. A solution of the tetra-aldehyde **14** (130 mg, 0.18 mmol) in dry THF (5 mL) was then added dropwise over 10 min. After 20 min, the mixture was heated to reflux and the reaction was conducted overnight under argon atmosphere. After cooling, the mixture was poured onto NH_4Cl (aq.) (30 mL) and the organic fraction was diluted with AcOEt (15 mL), extracted, washed with water (40 mL) and brine (40 mL), dried over Na_2SO_4 and evaporated to dryness. The residue was then chromatographed on silica using PE (2)/CH_2Cl_2(1) as eluent to provide the desired product **1** as a white solid (10 mg, 0.015 mmol, 8.5 %) after evaporation of the solvents. The two enantiomers were then separated using chiral HPLC (Chiralpak-IB–N column, *n*-heptane/CH_2Cl_2 95:5).

^{1}H NMR (600 MHz, $CDCl_3$, 25 °C): δ = 7.57–7.54 (m, 2H, H_{Ph}), 7.45–7.41 (m, 6H, H_{Ph}), 7.38 (dd, J = 7.7, 1.8 Hz, 2H, $H_{TP\text{-}b}$), 7.28 (dd, J = 7.7, 0.5 Hz, 2H, $H_{TP\text{-}b}$), 7.26–7.24 (m, 2H, H_{Ar}), 7.08–7.03 (m, 4H, $H_{TP\text{-}a}$ + H_{Ar}), 6.90–6.86 (m, 4H, $H_{TP\text{-}a}$ + H_{vinyl}), 6.78 (d, J = 10.8 Hz, 2H, H_{vinyl}), 6.50 (d, J = 1.7 Hz, 2H, $H_{TP\text{-}b}$), 6.27 (d, J = 1.7 Hz, 2H, $H_{TP\text{-}a}$), 6.10 (dd, J = 8.1, 1.9 Hz, 2H, H_{Ar}), 6.04 (dd, J = 8.1, 1.8 Hz, 2H, H_{Ar}). ^{13}C NMR (150 MHz, $CDCl_3$, 25 °C): δ = 141.51, 141.37, 141.36 (2 C), 140.98, 139.66, 139.40, 139.02, 137.92, 135.97, 133.54 (CH), 132.64 (CH), 130.63 (CH), 130.61 (CH), 130.05 (CH), 129.98 (CH), 129.61 (CH), 129.45 (CH), 128.70 (CH), 128.11 (CH), 127.97 (CH), 127.79 (CH), 127.69 (CH), 127.23 (CH), 127.13 (CH), 126.79 (CH). HR-MS (ESI-TOF), *m/z*: calc. for $C_{52}H_{32}Ag$ ($[M+Ag]^+$): 763.1549 ; Found: 763.1538. X-Ray: Crystals grown from dichloromethane/methanol; size: 0.30 × 0.30 × 0.20 mm. T = 150 K, monoclinic, space group $C2/c$, a = 13.7523 (3) Å, b = 13.5387 (3) Å, c = 18.8886 (4) Å, α = 90°, β = 98.660 (2)°, γ = 90°, V = 3476.74 (13) Å^3, Z = 4, θ(max) = 56.631°, $N_{reflexions}$ = 3476, R_1 = 0.0539 on 3065 reflections with $I \geq 2\sigma(I)$, wR_2 = 0.1532 on all data. UV-vis (chloroform, 20 °C), λ_{max} (ε): 229 (65960), 253 (59290), 290 nm (19320 L·mol^{-1}).

Synthesis of 1 from 15 (RCM strategy): To a solution of the tetravinylene **15** (50 mg, 70 μmol) in CH_2Cl_2 (100 mL) was added Hoveyda-Grubbs catalyst second-generation (9 mg, 14 μmol, 0.2 equiv). The mixture was then heated to reflux for 24 h. After evaporation of the solvents, the product was extracted by column chromatography on silica using PE/CH_2Cl_2 3:1. After evaporation of the solvents under reduced pressure, compound **1** (m = 42 mg, 64 μmol, 91 %) was obtained with similar analytical data as described for the transformation of product **14**.

Synthesis of 2: A solution of compound **1** (26 mg, 40 mmol) in dioxane (3.5 mL) containing cyclohexa-1,4-diene (0.6 mL) was bubbled with argon for 20 min in a Schlenk flask. Pd/C (10 %, 8.4 mg, 8.0 μmol, 0.2 equiv) was then added, the flask was sealed, and the temperature was raised to 90 °C. After 1 h, the mixture was cooled to room temperature, diluted with AcOEt and filtered over alumina. After evaporation of the solvents, the residue was purified by column chromatography using PE/CH_2Cl_2 2:1 on silica then by

chiral HPLC (chiralpak-IB–N column, *n*-heptane/CH_2Cl_2 90:10) to afford both enantiomers of **2** in equal amounts as white solids (m = 22 mg, 33 μmol, 84%). ^{1}H NMR (600 MHz, $CDCl_3$, 25 °C): δ = 7.52–7.49 (m, 2H, H_{Ph}), 7.41–7.35 (m, 4H, H_{Ph}), 7.34 (dd, J = 7.7, 1.8 Hz, 2H, $H_{TP\text{-}b}$), 7.33–7.30 (m, 2H, H_{Ph}), 7.22 (d, J = 7.7 Hz, 2H, $H_{TP\text{-}b}$), 7.12 (dd, J = 7.7, 2.0 Hz, 2H, H_{Ar}), 7.04–7.00 (m, 4H, $H_{TP\text{-}a}$ + H_{Ar}), 6.80 (d, J = 7.8 Hz, 2H, $H_{TP\text{-}a}$), 6.43 (d, J = 1.7 Hz, 2H, $H_{TP\text{-}b}$), 6.18–6.15 (m, 4H, H_{Ar} + $H_{TP\text{-}a}$), 5.97 (dd, J = 8.0, 1.8 Hz, 2H, H_{Ar}), 3.21–3.14 (m, 2H, CH_2), 3.10–3.03 (m, 2H, CH_2), 2.69–2.60 (m, 4H, CH_2). ^{13}C NMR (150 MHz, $CDCl_3$, 25 °C): δ = 142.14, 141.67, 141.26, 141.23, 141.20, 139.72, 138.91, 138.57, 138.54, 137.92, 130.28 (CH), 130.22 (CH), 129.53 (CH), 129.19 (2CH), 129.16 (CH), 128.11 (CH), 127.93 (CH), 127.50 (CH), 127.48 (2CH), 127.46 (CH), 126.73 (CH), 126.30 (CH), 36.25 (CH_2), 36.23 (CH_2). HR-MS (ESI-TOF), m/z: calc. for $C_{52}H_{36}Ag$ $[M+Ag]^+$: 767.1862; found: 767.1867. X-ray: Crystals grown from chloroform/methanol; size: 0.30 x 0.30 x 0.20 mm. T = 150 K, monoclinic, space group $P2_1/c$, a = 14.6050 (4) Å, b = 15.5266 (3) Å, c = 15.7816 (4) Å, α = 90°, β = 91.980 (2)°, γ = 90°, V = 3576.59 (15) Å^3, Z = 4, θ(max) = 56.711°, $N_{reflexions}$ = 7131, R_1 = 0.0468 on 5549 reflections with $I \geq 2\sigma(I)$, wR_2 = 0.1329 on all data. UV-vis (chloroform, 20 °C), λ_{max} (ε): 229 (51430), 240 (47730), 284 nm (8450 L·mol^{-1}).

Deposition Numbers 2087693 (**1**) and 2087694 (**2**) contain the supplementary crystallographic data for this paper. These data are provided free of charge by the joint Cambridge Crystallographic Data Centre and Fachinformationszentrum Karlsruhe Access Structures service.

Acknowledgements

Generous financial support by the Swiss National Science Foundation (SNF grants no. 200020-178808 and 51NF40-182895) is gratefully acknowledged. M.M. acknowledges support by the 111 project (90002-18011002). Calculations were performed at sciCORE (http://scicore.unibas.ch/) scientific computing core facility at University of Basel. Open access funding provided by CSAL.

Conflict of Interest

The authors declare no conflict of interest.

Keywords: bicycles · "Geländer" molecules · helical chirality · hydrocarbons · macrocyclization

[1] A. Link, C. Sparr, *Chem. Soc. Rev.* **2018**, *47*, 3804–3815.
[2] E. Yashima, N. Ousaka, D. Taura, K. Shimomura, T. Ikai, K. Maeda, *Chem. Rev.* **2016**, *116*, 13752–13990.
[3] M. Rickhaus, M. Mayor, M. Juríček, *Chem. Soc. Rev.* **2016**, *45*, 1542–1556.
[4] T. Leigh, P. Fernandez-Trillo, *Nature Rev. Chem.* **2020**, *4*, 291–310.
[5] Y. Yang, Y. Zhang, Z. Wei, *Adv. Mater.* **2013**, *25*, 6039–6049.
[6] G. Albano, G. Pescitelli, L. Di Bari, *Chem. Rev.* **2020**, *120*, 10145–10243.
[7] L. Pu, *MRS OPL* **1999**, *598*, BB5.3; DOI 10.1557/PROC-598-BB5.3.
[8] L. Pu, *Macromol. Rapid Commun.* **2000**, *21*, 795–809.
[9] Y. Yang, R. C. da Costa, M. J. Fuchter, A. J. Campbell, *Nat. Photonics* **2013**, *7*, 634–638.
[10] N. Chen, B. Yan, *Molecules* **2018**, *23*, 3376.
[11] H. Isla, J. Crassous, *C. R. Chim.* **2016**, *19*, 39–49.
[12] N. Y. Kim, J. Kyhm, H. Han, S. J. Kim, J. Ahn, D. K. Hwang, H. W. Jang, B.-K. Ju, J. A. Lim, *Adv. Funct. Mater.* **2019**, *29*, 1808668.
[13] Y. Kalachyova, O. Guselnikova, R. Elashnikov, I. Panov, J. Žádný, V. Církva, J. Storch, J. Sykora, K. Zaruba, V. Švorčík, O. Lyutakov, *ACS Appl. Mater. Interfaces* **2019**, *11*, 1555–1562.
[14] B. Göhler, V. Hamelbeck, T. Z. Markus, M. Kettner, G. F. Hanne, Z. Vager, R. Naaman, H. Zacharias, *Science* **2011**, *331*, 894–897.
[15] V. Kiran, S. P. Mathew, S. R. Cohen, I. H. Delgado, J. Lacour, R. Naaman, *Adv. Mater.* **2016**, *28*, 1957–1962.
[16] Y. Shen, C.-F. Chen, *Chem. Rev.* **2012**, *112*, 1463–1535.
[17] Y. Nakai, T. Mori, Y. Inoue, *J. Phys. Chem. A* **2013**, *117*, 83–93.
[18] T. Mori, *Chem. Rev.* **2021**, *121*, 2373–2412.
[19] Y. Nakakuki, T. Hirose, H. Sotome, H. Miyasaka, K. Matsuda, *J. Am. Chem. Soc.* **2018**, *140*, 4317–4326.
[20] G. R. Kiel, K. L. Bay, A. E. Samkian, N. J. Schuster, J. B. Lin, R. C. Handford, C. Nuckolls, K. N. Houk, T. D. Tilley, *J. Am. Chem. Soc.* **2020**, *142*, 11084–11091.
[21] N. J. Schuster, L. A. Joyce, D. W. Paley, F. Ng, M. L. Steigerwald, C. Nuckolls, *J. Am. Chem. Soc.* **2020**, *142*, 7066–7074.
[22] R. H. Martin, M. J. Marchant, *Tetrahedron* **1974**, *30*, 347–349.
[23] H. Kubo, T. Hirose, T. Nakashima, T. Kawai, J. Hasegawa, K. Matsuda, *J. Phys. Chem. Lett.* **2021**, *12*, 686–695.
[24] B. Kiupel, C. Niederalt, M. Nieger, S. Grimme, F. Vögtle, *Angew. Chem. Int. Ed.* **1998**, *37*, 3031–3034; *Angew. Chem.* **1998**, *110*, 3206–3209.
[25] M. Rickhaus, L. M. Bannwart, M. Neuburger, H. Gsellinger, K. Zimmermann, D. Häussinger, M. Mayor, *Angew. Chem. Int. Ed.* **2014**, *53*, 14587–14591; *Angew. Chem.* **2014**, *126*, 14816–14820.
[26] M. Rickhaus, L. M. Bannwart, O. Unke, H. Gsellinger, D. Häussinger, M. Mayor, *Eur. J. Org. Chem.* **2015**, 786–801.
[27] M. Rickhaus, O. T. Unke, R. Mannancherry, L. M. Bannwart, M. Neuburger, D. Häussinger, M. Mayor, *Chem. Eur. J.* **2015**, *21*, 18156–18167.
[28] R. Mannancherry, M. Rickhaus, D. Häussinger, A. Prescimone, M. Mayor, *Chem. Sci.* **2018**, *9*, 5758–5766.
[29] R. Mannancherry, T. Šolomek, D. Cavalli, J. Malinčík, D. Häussinger, A. Prescimone, M. Mayor, *J. Org. Chem.* **2021**, *86*, 5431–5442.
[30] P. Rashidi-Ranjbar, Y. M. Man, J. Sandstroem, H. N. C. Wong, *J. Org. Chem.* **1989**, *54*, 4888–4892.
[31] H. Huang, T. Stewart, M. Gutmann, T. Ohhara, N. Niimura, Y.-X. Li, J.-F. Wen, R. Bau, H. N. C. Wong, *J. Org. Chem.* **2009**, *74*, 359–369.
[32] J.-W. Han, J.-X. Chen, X. Li, X.-S. Peng, H. N. C. Wong, *Synlett* **2013**, *24*, 2188–2198.
[33] J.-W. Han, X.-S. Peng, H. N. C. Wong, *Natl. Sci. Rev.* **2017**, *4*, 892–916.
[34] F. Lin, H.-Y. Peng, J.-X. Chen, D. T. W. Chik, Z. Cai, K. M. C. Wong, V. W. W. Yam, H. N. C. Wong, *J. Am. Chem. Soc.* **2010**, *132*, 16383–16392.
[35] J.-X. Chen, J.-W. Han, H. N. C. Wong, *Org. Lett.* **2015**, *17*, 4296–4299.
[36] J. E. McMurry, M. P. Fleming, *J. Am. Chem. Soc.* **1974**, *96*, 4708–4709.
[37] M. Ephritikhine, *Chem. Commun.* **1998**, 2549–2554.
[38] R. H. Grubbs, *Tetrahedron* **2004**, *60*, 7117–7140.
[39] G. Wittig, U. Schöllkopf, *Chem. Ber.* **1954**, *87*, 1318–1330.
[40] G. Wittig, W. Haag, *Chem. Ber.* **1955**, *88*, 1654–1666.
[41] N. Miyaura, A. Suzuki, *Chem. Rev.* **1995**, *95*, 2457–2483.
[42] N. Miyaura, K. Yamada, A. Suzuki, *Tetrahedron Lett.* **1979**, *20*, 3437–3440.
[43] C. Zhu, Y. Zhao, D. Wang, W.-Y. Sun, Z. Shi, *Sci. Rep.* **2016**, *6*, 33131.
[44] W. Li, J. Li, D. DeVincentis, T. S. Mansour, *Tetrahedron Lett.* **2004**, *45*, 1071–1074.
[45] A. Pradhan, P. Dechambenoit, H. Bock, F. Durola, *Chem. Eur. J.* **2016**, *22*, 18227–18235.
[46] T. Mukaiyama, T. Sato, J. Hanna, *Chem. Lett.* **1973**, *2*, 1041–1044.
[47] H. R. Darabi, A. D. Farahani, M. H. Karouei, K. Aghapoor, R. Firouzi, R. Herges, A. R. Mohebbi, C. Näther, *Supramol. Chem.* **2012**, *24*, 653–657.
[48] S. B. Garber, J. S. Kingsbury, B. L. Gray, A. H. Hoveyda, *J. Am. Chem. Soc.* **2000**, *122*, 8168–8179.
[49] S. Gessler, S. Randl, S. Blechert, *Tetrahedron Lett.* **2000**, *41*, 9973–9976.
[50] M. C. Bonifacio, C. R. Robertson, J.-Y. Jung, B. T. King, *J. Org. Chem.* **2005**, *70*, 8522–8526.
[51] J. F. Quinn, D. A. Razzano, K. C. Golden, B. T. Gregg, *Tetrahedron Lett.* **2008**, *49*, 6137–6140.
[52] M. Fujiki, J. R. Koe, T. Mori, Y. Kimura, *Molecules* **2018**, *23*, 2606.
[53] K. Sato, M. Hasegawa, Y. Nojima, N. Hara, T. Nishiuchi, Y. Imai, Y. Mazaki, *Chem. Eur. J.* **2021**, *27*, 1323–1329.

Manuscript received: June 4, 2021
Accepted manuscript online: July 13, 2021
Version of record online: August 5, 2021

